DECAY OF STRONG PLANE SHOCKS IN AN IDEAL GAS

By Pei Chi Chou, Robert R. Karpp, and Lawrence J. Zajac

Prepared under Contract No. NsG-270-63 by
DREXEL INSTITUTE OF TECHNOLOGY
Philadelphia, Pa.

for

NATIONAL AERONAUTICS AND SPACE ADMINISTRATION

For sale by the Office of Technical Services, Department of Commerce,
Washington, D.C. 20230 -- Price $1.25

DECAY OF STRONG PLANE SHOCKS IN AN IDEAL GAS

by Pei Chi Chou, Robert R. Karpp, and Lawrence J. Zajac

DREXEL INSTITUTE OF TECHNOLOGY

29204

ABSTRACT

An approximate analytical solution for the decay of strong plane shocks in an ideal gas is developed as the first step in the study of spherical shocks produced by hypervelocity impact. A graphical solution to the same problem is obtained by a stepwise characteristics method in order to establish a criterion with which to compare the present analytical solution. Although it is based upon certain simplifying assumptions, the analytical solution yields a good time-history representation of the shock wave phenomena in an ideal gas. For weak shocks, both the analytical and graphical solutions agree favorably with Friedrichs' solution at small values of time. By a modification of the equation of state, the approximation technique developed in this report can be extended to other media.

Author

TABLE OF CONTENTS

LIST OF FIGURES

LIST OF TABLES

DECAY OF STRONG PLANE SHOCKS IN AN IDEAL GAS

I. Introduction:

The shock front created by hypervelocity impact in a liquid is very close to hemispherical in shape as evidenced by the experiments performed by Stepka.[1] In a previous report,[2] based upon the spherical symmetry of the shock front, the authors have developed an approximate semi-empirical equation which gives the time-history of the peak pressure behind the shock front. Other investigators[3,4] have also attempted to investigate the spherical shock in liquids or solids by analytical methods; however, no conclusive results have been obtained. These analytical approaches, which are based upon certain similarity assumptions first made by G. I. Taylor, yield good results in the solution of blast waves in air, but so far they have not proved satisfactory for the solution of impact problems. Since the pure analytical approach has not been successful, it is desirable to employ numerical methods.

Two such numerical methods that may be employed for the calculation of the decay of shock waves are the finite-difference method and the characteristics method. The finite-difference method is more convenient for computer calculation, but at times its accuracy is inferior, especially in the region bordering the shock front.[5] Therefore, in the present problem, where the peak pressure and the exact path are desired, the characteristics method will be employed.

There are two factors which govern the decay of three-dimensional (or two-dimensional) strong shocks--

1. The effect of the space dispersion and
2. the interaction between the shock front and the rarefaction waves originating from free surfaces.

The latter of these two (the rarefaction wave effect) can best be studied by the decay behavior of plane shocks. In this report, the decay of plane shocks is studied by the characteristic method, which is considered to be the first step in the analysis of the spherical shock problem.

Al'tshuler and his coworkers[6] have calculated the decay of strong plane shocks in certain special cases by the stepwise characteristics method. However, the results have not been reported in detail, nor has any approximate analytical expression for the shock path been obtained. In the case of weak shocks in an ideal gas, Friedrichs derived approximate equations for the shock path by the method of characteristics.[7] The accuracy of Friedrichs' method was later studied by Lighthill.[8] Fowles likewise obtained similar equations for the decay of weak shocks in solids or liquids with the Murnaghan equation of state[9] by assuming the weak shocks to be isentropic compressions.

By following an analytical approach similar to the one used by Friedrichs, we have obtained an approximate equation for the shock path of a strong shock in an ideal gas. The characteristics method using a stepwise graphical scheme has also been applied to the same problem, and the results compared with the approximate analytical solutions with excellent agreement. With a slight modification of the equation of state, the method developed in this report can be easily applied to a liquid or solid medium.

In the analytical approach, it is assumed that the reflected waves and contact lines resulting from the interaction between a rarefaction wave and a strong shock are weak and can therefore be neglected. Across the shock front, exact shock conditions are used instead of the approximate shock conditions used by Friedrichs.

It is interesting to note that for weak shocks, according to Friedrichs' solution, the distance between the shock front and rarefaction tail (width of the shock wave) increases as the square root of time for large values of time.

According to the present solution, the width of the shock wave reduces to zero at some finite, although large, time. This inconsistancy in solutions is described in Section VI. The exact position of the tail of the rarefaction wave is found to lie between the tail predicted by the present approximation and the tail predicted by Friedrichs' approximation.

In this report, the precise problem to be solved is first stated and then Friedrichs' existing solution for weak shocks is summarized. A derivation of the present approximate anaytical solution for strong shocks is presented along with the necessary simplifying assumptions. A summary of the method of characteristics pertinent to the solution of the present problem follows. Then the procedure for a solution by the stepwise characteristics method is presented along with a new graphical scheme utilizing a modified state plane. The accuracy of the present analytical solution is next studied by approximately determining the errors introduced by the simplifying assumptions. A detailed comparison of the three solutions (Friedrichs' solution for weak shocks, the present anaytical solution, and the stepwise characteristics solution) is made for shocks of different strengths. A discussion of the behavior of weak shocks according to the two approximate analytical solutions is next given. The report is concluded with statements on the significance and possible extensions of the approximation procedure developed herein.

II. Statement of Problem

The problem to be studied is identical with one treated by Friedrichs.[7] It consists of a semi-infinite tube containing an initially stagnant, ideal gas under the influence of a piston operating at the closed end. The piston is first accelerated to a constant velocity; then, after a small displacement, it is suddenly arrested and thereafter remains motionless, as shown in figure 1.

The instantaneous acceleration of the piston into the gas produces a shock wave of constant strength and velocity. The sudden arresting of the piston, at the point (x_1, t_1) in the x-t plane, produces a centered simple rarefaction wave emanating from that point. The head of the rarefaction wave, which is travelling at a greater speed than the shock, eventually overtakes the shock front at (x_2, t_2) where an interaction between the two waves takes place. Consequently, the shock velocity and the pressure ratio deteriorate in magnitude and strength.

A complete solution of the problem involves the determination of the path of the shock front in the x-t plane and a description of the state of the gas behind the shock.

III. Friedrichs' Solution for Weak Shocks

As illustrated by Friedrichs, his solution is accurate for weak or moderate shocks with excess pressure ratios of 1.5 or less.[7] His solution is summarized below since it will be used later for purposes of comparison.

The approximations upon which his method is based are obtained by neglecting shock strength terms of third order or higher. As a consequence, the change in entropy across the shock front is ignored. One may then disregard the "back reaction" of the shock on the wave motion if the conservation laws across the shock are appropriately modified. Using the above approximations, Friedrichs determined the following equation for the path of the shock front in the x-t plane.

$$x - x_1 = c_1 (t - t_1) \; \frac{(t-t_1)^{1/2} + 5K(t_2-t_1)^{1/2}}{(t-t_1)^{1/2} + K(t_2-t_1)^{1/2}} \qquad (1)$$

for $t > t_2$

where $$K = \frac{u_2}{\frac{8}{\gamma+1} c_1 - u_2}$$

For time $t<t_2$, the shock motion is represented by the straight line

$$x = U_1 t \tag{2}$$

where $$U_1 = c_1\left[1+\frac{1}{2}\left(\frac{(\gamma+1)u_2}{2c_1}\right)+\frac{1}{8}\left(\frac{(\gamma+1)u_2}{2c_1}\right)^2\right]$$

Also, the excess pressure ratio at large times approaches the following expression asymptotically,

$$\frac{p-p_1}{p_1} = \frac{2\gamma}{\gamma+1}\left[4K\left(\frac{t_2-\tau_1}{t-\tau_1}\right)^{1/2}+4K^2\left(\frac{t_2-\tau_1}{t-\tau_1}\right)\right] , \tag{3}$$

and the pressure distribution over the wave zone, for large values of time, is approximately given by

$$\frac{p-p_1}{p_1} = \frac{2\gamma}{\gamma+1}\left[\frac{x-x_1}{c_1(t-t_1)}-1+\frac{1}{2}\left(\frac{x-x_1}{c_1(t-t_1)}-1\right)^2\right] . \tag{4}$$

An analysis of the accuracy of Friedrichs' method applied to strong shocks will be presented in section (V).

IV. Present Solutions for Strong Shocks

1. Governing Equations for Shocks and Isentropic Waves

The exact equations governing the fluid properties across a right-travelling shock are

$$\frac{u_2-u_1}{c_1} = \frac{2}{\gamma+1}\left(\frac{U}{c_1}-\frac{c_1}{U}\right) \tag{5}$$

$$\left(\frac{c_2}{c_1}\right)^2 = 1+\frac{2(\gamma-1)}{(\gamma+1)^2}\left[\gamma\left(\frac{U}{c_1}\right)^2-\left(\frac{c_1}{U}\right)^2-(\gamma-1)\right] \tag{6}$$

$$\frac{\rho_2}{\rho_1} = \frac{1}{1-\frac{2}{\gamma+1}\left[1-\left(\frac{c_1}{U}\right)^2\right]} \tag{7}$$

$$\frac{p_2}{p_1} = 1+\frac{2\gamma}{\gamma+1}\left[\left(\frac{U}{c_1}\right)^2-1\right] , \tag{8}$$

where all velocities are referred to ground. Subscripts 1 and 2 refer respectively to the fluid properties ahead of and behind the shock front. Equations (5) through (8) are derived from the continuity, momentum and energy equations, and the equation of state of an ideal gas.[11] Application of the theory of characteristics to the partial differential equation governing unsteady, one-dimensional, constant area, isentropic flow yields the following characteristic relationships

$$\frac{dx}{dt} = u \pm c \tag{9}$$

$$\frac{dc}{du} = \pm \frac{\gamma-1}{2} \tag{10}$$

where the upper and lower signs refer respectively to waves travelling to the right and left relative to the fluid. For regions of constant entropy, the pressure and sound speed are related by the following isentropic equation.

$$\frac{c}{c_o} = \left(\frac{p}{p_o}\right)^{\frac{\gamma-1}{2\gamma}} \tag{10a}$$

2. Approximate Analytical Solution for Strong Shocks

a. General Discussion

To develop an analytical solution for strong shocks, it is necessary to make certain basic symplifying assumptions. For weak or moderate shocks, Friedrichs neglects the change in entropy across the shock front and assumes that the simple wave behind the front is unaffected by the shock. For strong shocks, however, the entropy change across the shock is appreciable and can no longer be neglected. Fortunately, the reflected wave system is much weaker than the original shock or the original rarefaction wave. Consequently, our approach utilizes the exact shock conditions, equations (5) through (8), but with the simplifying approximations that:

1. in the original rarefaction wave, characteristic lines remain straight lines and that

2. the particle velocity u along any one of these characteristic lines remains constant.

With these assumed values of particle velocity u and the exact equations across the shock, the path of the shock front can be determined. For points directly behind the front, the sound speed as calculated from the exact shock equation (6) is different from the sound speed on the same straight characteristic line near point (x_1, t_1). Therefore, in the wave zone behind the shock front, the present approach results in an inconsistency in sound speed (and pressure). Consequently, the exact shock equations are used to calculate sound speeds and pressures at points just behind the shock front. But the sound speeds and pressures at points on the tail of the rarefaction wave are computed by the characteristic equations, and a linear variation in properties between the shock front and rarefaction tail is assumed.

The present assumptions introduce very slight errors in the early stage of the propagation of the shock front because the rarefaction wave has undergone only small deflections caused by the shock-rarefaction interactions. For later stages, however, greater errors are introduced since greater deflections are encountered.

b. Development of Equations

In the present problem, the particle velocity u ahead of the shock front is zero. Therefore, equation (5) can be rearranged to yield the following relationship between shock propagation velocity U and gas particle velocity u.

$$U = \frac{\gamma+1}{4} u + \left[\left(\frac{\gamma+1}{4} \right)^2 u^2 + c_1^2 \right]^{1/2}, \tag{11}$$

where the subscript notation corresponds to figure 1. Using assumption (1) of the preceding section and equation (9), the following equation of the straight

characteristic lines within the rarefaction wave, centered at (x_1, t_1), can be obtained.

$$x - x_1 = (u + c)(t - t_1) \tag{12}$$

The integrated form of equation (10) is

$$c - c_2 = \frac{\gamma-1}{2}(u - u_2) \ , \tag{13}$$

which is the relationship between sound speed and particle velocity across a right travelling isentropic wave. Combining equations (12) and (13), one obtains

$$x - x_1 = \left(\frac{\gamma+1}{2}u + c_2 - \frac{\gamma-1}{2}u_2\right)(t - t_1) \ . \tag{14}$$

The differential form of equation (14) is

$$\frac{dx}{du} = \frac{\gamma+1}{2}(t - t_1) + \left(\frac{\gamma+1}{2}u + c_2 - \frac{\gamma-1}{2}u_2\right)\frac{dt}{du} \tag{15}$$

where the differentiation is taken with respect to u. For the path of the shock front,

$$\frac{dx}{dt} = U$$

and

$$\frac{dx}{du} = \frac{dx}{dt}\frac{dt}{du} = U\frac{dt}{du} \ . \tag{16}$$

Substituting equation (16) into (15), and using equation (11) and assumption 2, one obtains the following differential equation relating u and t.

$$\left[\left[\left(\frac{\gamma+1}{4}\right)^2 u^2 + c_1^2\right]^{1/2} - \frac{\gamma+1}{4}u - c_2 + \frac{\gamma-1}{2}u_2\right]dt = (t - t_1)\frac{\gamma+1}{2}du \tag{17}$$

Equation (17) may be integrated, with limits t_2 to t and u_2 to u, and then the following equations may be presented.

$$t - t_1 = (t_2 - t_1)\exp\left\{-c_1^2\left[\frac{1}{c_3}\left(\frac{1}{Z} - \frac{1}{Z_1}\right) + \left(\frac{1}{c_3^2} + \frac{1}{c_1^2}\right)\ln\left|\frac{Z - c_3}{Z_1 - c_3}\right| + \frac{1}{c_3^2}\ln\left|\frac{Z_1}{Z}\right|\right]\right\} \tag{18}$$

$$x - x_1 = \left(\frac{\gamma+1}{2}u + c_3\right)(t - t_1) \ , \tag{14}$$

where $$c_3 = c_2 - \frac{\gamma-1}{2} u_2$$

$$z = \left[\left(\frac{\gamma+1}{4}\right)^2 u^2 + c_1^2\right]^{1/2} - \frac{\gamma+1}{4} u$$

$$z_1 = \left[\left(\frac{\gamma+1}{4}\right)^2 u_2^2 + c_1^2\right]^{1/2} - \frac{\gamma+1}{4} u_2 \quad ,$$

and c_2 is calculated from equations (5) and (6). Equations (14) and (18) describe the path of the shock front in terms of the parameter u, for time $t>t_2$. For time $o<t<t_2$, the shock path is the straight line $x= U_1 t$, where U_1 is obtained from equation (11) with $u= u_2$.

An equation for the shock velocity U as a function of x and t can be obtained from equations (11) and (14).

$$U = \frac{1}{2}\left(\frac{x-x_1}{t-t_1} - c_3\right) + \left[\frac{1}{4}\left(\frac{x-x_1}{t-t_1} - c_3\right)^2 + c_1^2\right]^{1/2} \qquad (19)$$

for $t>t_2$ and $x>x_2$. The constant shock velocity, for $o<t<t_2$, is, from equation (11)

$$U_1 = \frac{\gamma+1}{4} u_2 + \left[\left(\frac{\gamma+1}{4}\right)^2 u_2^2 + c_1^2\right]^{1/2}. \qquad (20)$$

By combining equation (19) with equation (8), one may obtain the following expression for the excess pressure ratio across the shock front, for $t>t_2$,

$$\frac{p-p_1}{p_1} = \frac{2\gamma}{\gamma+1}\left\{\left[\frac{1}{2c_1}\left(\frac{x-x_1}{t-t_1} - c_3\right) + \left[\frac{1}{4c_1^2}\left(\frac{x-x_1}{t-t_1} - c_3\right)^2 + 1\right]^{1/2}\right]^2 - 1\right\} \qquad (21)$$

3. Graphical Solution by the Method of Characteristics

a. General Discussion

Since no exact analytical solution for strong shocks exists, some criterion must be established against which the present solution may be compared. The method of characteristics by stepwise calculations usually yields good results, but it is normally quite lengthly.[10, 11] However, the use of a new graphical

technique reduces the amount of time required for a solution by this method. This technique utilizes a $(p/p_1)^{\frac{\gamma-1}{2\gamma}}$ versus (u/c_1) state plane instead of the conventional (c/c_1) versus (u/c_1) state plane. The basic problem is solved by this stepwise characteristics method, and the results are compared with the analytical solution for strong shocks.

The partial differential equation describing unsteady, one-dimensional, constant area, isentropic flow is hyperbolic in nature and can be solved numerically by the stepwise characteristics method. The method utilizes two planes, the physical plane ($c_1 t$-x diagram of figure 2) and the state plane (c/c_1 - u/u_1 diagram of figure 3a). In applying the stepwise characteristics method, one replaces a region with continuously varying fluid properties in the physical plane by a number of smaller regions, each having uniform fluid properties. (thus, the "field method" adaptation of the characteristics method has been used as opposed to the "lattice point method".)[11] The graphical solution is then obtained by constructing the complete flow field in the physical and state planes.

Since the fluid remains in contact with the piston face, the initial portion of the shock and rarefaction waves may be constructed in the physical plane, (see figure 2). The initial shock velocity U_1 is calculated from equation (20) with u_2 equal to the piston velocity, and then the initial portion of the shock front with slope c_1/U_1 is constructed. The simple rarefaction wave centered at $(x_1, c_1 t_1)$ may be arbitrarily divided into six regions by assuming approximately equal increments of particle velocity between adjacent regions. The initial portion of the rarefaction wave is then constructed, by noting that the I-characteristics (right-travelling waves) have slopes given by

$$\left(\frac{d(c_1 t)}{dx}\right)_I = \frac{c_1}{u+c} \qquad (9')$$

where u and c are now the average between the values on both sides of the characteristics line. These waves are propagated with constant strength until the head of the rarefaction wave overtakes the shock front. An interaction between the waves then follows; and, as the shock continues with decreased strength and velocity, a contact line in addition to the reflected wave is formed. The shock strength diminishes as the difference in particle velocity across the front is reduced. A contact line, which separates regions of unequal entropy, forms because fluid particles passing through shocks of unequal strengths attain different levels of entropy. A reflected wave is required in order to satisfy the boundary conditions of equal pressure and equal particle velocity across a contact line.

The remainder of the physical plane may be constructed by repeating a few unit operations presented in the following section.

b. Unit Operations for Wave Interactions

Interaction of Shock and Rarefaction Waves

The fluid properities in regions 1, 2 and 4 are completely known from the initial conditions of the problem, (see figure 2). The determination of the fluid properties in regions 10 and 20 represents a typical unit operation for the interaction of shock and rarefaction waves. The particle velocity and pressure in regions 10 and 20 must be equal since the regions are separated by a contact line, thus

$$u_{10} = u_{20} \tag{22}$$

and

$$p_{10} = p_{20} \ . \tag{23}$$

The process from region 4 to region 10 is isentropic; therefore, according to equation (10a),

$$\frac{c_{10}}{c_4} = \left(\frac{p_{10}}{p_4}\right)^{\frac{\gamma-1}{2\gamma}} \ . \tag{24}$$

Also, the change in fluid properties across a left-travelling isentropic wave (region 4 to region 10) is, from equation (10),

$$c_{10} - c_4 = -\frac{\gamma-1}{2}(u_{10} - u_4) \tag{25}$$

The shock relations governing the change from region 1 to region 20 are

$$\frac{u_{20}}{c_1} = \frac{2}{\gamma+1}\left(\frac{U}{c_1} - \frac{c_1}{U}\right) \tag{26}$$

$$\left(\frac{c_{20}}{c_1}\right)^2 = 1 + \frac{2(\gamma-1)}{(\gamma+1)^2}\left[\gamma\left(\frac{U}{c_1}\right)^2 - \left(\frac{c_1}{U}\right)^2 - (\gamma-1)\right] \tag{27}$$

and

$$\frac{p_{20}}{p_1} = 1 + \frac{2\gamma}{\gamma+1}\left[\left(\frac{U}{c_1}\right)^2 - 1\right] \tag{28}$$

Equations (22) to (28) represent a system of seven simultaneous equations which may be solved for the unknowns U, p_{10}, p_{20}, u_{10}, u_{20}, c_{10}, and c_{20}, thereby determining the fluid properties of regions 10 and 20. However, to solve these equations requires a trial and error procedure which is time consuming;* therefore, a new graphical method for the solution of these equations, to be explained in section c, has been developed.

Interaction of Isentropic Waves and Contact Lines

When an isentropic wave (a right or left travelling characteristic) intersects a contact line, it is in general necessary to have both reflected and transmitted waves. For example, the characteristic dividing regions 10 and 11 in figure 2 intersects the first contact line. The fluid properties in regions 21 and 30 may then be determined from the known properties of regions 10, 11, and 20. The fluid particle velocity and pressure on both sides of the contact line (regions 21 and 30)

*See, for instance, pages 202-203, ref. 10, or page 1026, ref. 11.

must be equal, or

$$u_{21} = u_{30} \tag{29}$$

and

$$p_{21} = p_{30} \tag{29'}$$

Since the isentropic relation is valid for regions on the same side of a contact line, equation (29') may be presented as

$$\frac{c_{21}}{c_{10}} = \frac{c_{30}}{c_{20}} \tag{30}$$

The relationships between fluid properties across isentropic waves, for the regions under consideration, are

$$c_{21} - c_{11} = -\frac{\gamma-1}{2}(u_{21} - u_{11}) \tag{31}$$

$$c_{30} - c_{20} = \frac{\gamma-1}{2}(u_{30} - u_{20}) \tag{32}$$

This system of four simultaneous equations (equations 29, 30, 31, and 32) may be solved for the four unknowns: c_{21}, c_{30}, u_{21}, u_{30}, which completely determine regions 21 and 30. A graphical method, to be presented in the next section, is also available for the solution of these equations.

c. Graphical Solutions for Wave Interactions:

To facilitate construction of the physical plane, it is advantageous to apply a graphical method to solve the aforementioned equations governing wave interactions. Due to the stepwise continuous construction, regions in the physical plane map into points in the state plane (see figures 2 and 3). The conditions of equal pressure and equal particle velocity across a contact line suggest plotting the characteristics on a p-u state plane.

By integrating equation (10), with limits c_n to c and u_n to u, where the subscript designates a reference region in which the fluid properties are known, and dividing by c_1, one may obtain the equations of the characteristics in the

c/c_1 - u/c_1 plane.

$$\frac{c}{c_1} = \frac{c_n}{c_1} \pm \frac{\gamma-1}{2}\left(\frac{u}{c_1} - \frac{u_n}{c_1}\right) \tag{33}$$

Subscript 1 refers to the region ahead of the shock, and the process from condition (c, u) to condition (c_n, u_n) must be isentropic. The following equation may be derived from equation (10a).

$$\frac{c}{c_1} = \left(\frac{p_1}{p_n}\right)^{\frac{\gamma-1}{2\gamma}}\left(\frac{c_n}{c_1}\right)\left(\frac{p}{p_1}\right)^{\frac{\gamma-1}{2\gamma}} \tag{34}$$

The equations of the p-u state characteristics, as shown below, may now be derived by combining equations (33) and (34).

$$\left(\frac{p}{p_1}\right)^{\frac{\gamma-1}{2\gamma}} = \pm\frac{\gamma-1}{2}\left(\frac{p_n}{p_1}\right)^{\frac{\gamma-1}{2\gamma}}\left(\frac{c_1}{c_n}\right)\frac{u}{c_1} + \left(\frac{p_n}{p_1}\right)^{\frac{\gamma-1}{2\gamma}}\left(\frac{c_1}{c_n}\right)\left[\frac{c_n}{c_1} \mp \frac{\gamma-1}{2}\left(\frac{u_n}{c_1}\right)\right] \tag{35}$$

The upper and lower signs refer respectively to characteristics of family II (changes across right-traveling waves) and family I (changes across left-travelling waves). The general practice for a graphical solution is to use the p-u state plane in which the characteristics given by equation (35) are curved lines.[11] Since many of these lines must be used for the graphical solution of the present problem, it is not convenient to plot them in the p-u plane. It is convenient, however, to use a $(p/p_1)^{\frac{\gamma-1}{2\gamma}}$ vs. (u/c_1) modified state plane in which the characteristics are straight lines. Figure 3b illustrates the modified state plane with u/c_1 as the abscissa and $(p/p_1)^{\frac{\gamma-1}{2\gamma}}$ as the ordinate. In this plane, equations (35) represent two families of straight lines with slopes $\pm\frac{\gamma-1}{2}(p_n/p_1)^{\frac{\gamma-1}{2\gamma}}(c_1/c_n)$. By using the isentropic relationship, equation (10a), it can be shown that for regions of constant entropy the slope of equations (35) remains constant. For example,

$$\frac{\gamma-1}{2}\left(\frac{p_2}{p_1}\right)^{\frac{\gamma-1}{2\gamma}}\left(\frac{c_1}{c_2}\right) = \frac{\gamma-1}{2}\left(\frac{p_4}{p_1}\right)^{\frac{\gamma-1}{2\gamma}}\left(\frac{c_1}{c_4}\right)$$

where the isentropic relationship $(p_2 / p_4)^{\frac{\gamma-1}{2\gamma}} = c_2 / c_4$ is valid from region 2 to region 4.

The shock polar, a graphical representation of the shock relationships, can also be plotted in the $(p/p_1)^{\frac{\gamma-1}{2\gamma}}$ versus (u/c_1) state plane from equations (5) and (8). Since only one shock polar is needed for the present problem, the fact that it is a curved line does not introduce any inconvenience. Using the shock polar and state characteristics in the $(p/p_1)^{\frac{\gamma-1}{2\gamma}}$ versus (u/c_1) state plane it is possible to solve for fluid properties graphically in regions created by the wave interactions.

Interaction of Shock and Rarefaction Waves

The seven equations relating fluid properties after the initial shock-rarefaction interaction (section IV-3b) can be solved graphically with the use of the $(p/p_1)^{\frac{\gamma-1}{2\gamma}}$ versus (u/c_1) state plane. With the fluid properties in regions 1, 2, and 4 known, it is possible to determine the fluid properties in regions 10 and 20 by the following graphical procedure.

Region 2 lying on the shock polar and region 4 lying on a II-characteristic with slope $+\frac{\gamma-1}{2}(p_2/p_1)^{\frac{\gamma-1}{2\gamma}}(c_1/c_2)$ and passing through point 2 are plotted in the state plane of figure 3b. Region 10 may be reached from region 4 by passing along a I-characteristic with slope $-\frac{\gamma-1}{2}(p_2/p_1)^{\frac{\gamma-1}{2\gamma}}(c_1/c_2)$. The shock polar represents all states immediately behind the shock front; therefore, region 20 must be a point on the shock polar. Because of the boundary conditions across a contact line, regions 10 and 20 map into the same point in the modified p-u state plane. Therefore, the intersection of the I-characteristic through point 4 and the shock polar locates region 10 and 20. The shock front propagation velocity can be directly determined from equation (11) with u_{20} substituted for u. All other regions about a rarefaction -shock interaction may be located in the state plane by an analogous procedure with suitable substitution made for p_2 and c_2.

Interaction of an Isentropic Wave and a Contact Line

The four equations relating fluid properties in regions about the intersection of a rarefaction wave and a contact line can also be solved graphically through the use of the modified p-u state plane. With known fluid properties in regions 10, 11, and 20, it is possible to graphically determine the fluid properties in regions 21 and 30 as follows.

Regions 10 and 11 which lie on the same II-characteristic with slope $+\frac{\gamma-1}{2}(p_2 / p_1)^{\frac{\gamma-1}{2\gamma}}(c_1 / c_2)$ may be plotted in the state plane of figure 3. Region 21 may be reached from region 11 by passing along a I-characteristic with slope $-\frac{\gamma-1}{2}(p_2 / p_1)^{\frac{\gamma-1}{2\gamma}}(c_1 / c_2)$, and region 30 may be reached from region 20 by passing along a II-characteristic of slope $+\frac{\gamma-1}{2}(p_{20} / p_1)^{\frac{\gamma-1}{2\gamma}}(c_1 / c_{20})$. Because of the boundary conditions across a contact line, regions 21 and 30 map into the same point in the modified p-u state plane. Therefore, the intersection of these characteristic lines locates regions 21 and 30. Note that the slope of a II-characteristic passing through point 10 is different from the slope of a II-characteristic passing through point 20, even though points 10 and 20 map into the same point in figure 3b. This difference is caused by the entropy change across the contact line dividing regions 10 and 20. All other regions about a characteristic line and contact line intersection may be located in the state plane by an analogous procedure provided proper substitution is made for the state variables.

d. Examples

Numerical examples for the present problem were obtained by applying the above procedures. For the numerical calculations, the following values of parameters were chosen.

$u_1 = 0$ $\gamma = 1.4$

$c_1 = 1128$ ft/sec piston travel $x_1 = 1$ ft.

$p_1 = 1$ atm

The following three problems were solved in detail.

prob.	initial shock strength	piston velocity u_2 ft/sec	initial excess pressure ratio $\frac{p_2 - p_1}{p_1}$	extent of graphical solution-final excess pressure ratio $\frac{p - p_1}{p_1}$	DIT drawing number
1	weak	200	0.274	0.200	1603
2	strong	2000	6.264	2.434	1601
3	very strong	18000	428.9	144.9	1602

The physical plane for problem 2 (strong shock) is shown in figure 2, and the state properties for several regions are given in table 1. Notice that some waves which are reflected from the contact lines are of negligible strength and therefore are not shown in the physical plane.

Graphical solutions for the path of the shock front in the physical plane are shown in figure 4 for all three problems.

V. Accuracy of Solutions

1. Accuracy of Assumptions

The simplifying assumptions made in Section IV-2 introduce errors of unknown magnitude into the present analytical solution. These inaccuracies cannot be calculated directly because no exact solution exists; however, an attempt to determine the order of magnitude of the errors was made and is given below.

Assumption (1) states that the characteristics are straight lines within the rarefaction wave. To verify this assumption, shock waves of three different

initial strengths (weak, strong, and very strong) were analyzed. For each case three positions within the rarefaction wave were considered; namely, head ($u = u_2$), middle ($u = 1/2\ u_2$), and tail ($u = o$). The slope of a characteristic line within the simple rarefaction wave was calculated first from equation (9) with appropriate values of u and c. Then, using the same value of u, the slope of a characteristic directly behind the shock front was calculated from equations (5), (6), and (9). The difference between these two slopes was used as the approximate deviation of the characteristic curves from a straight line. It should be mentioned that the characteristic directly behind the shock front is not a continuation of the characteristic within the simple rarefaction wave, but it is another characteristic with the same velocity (u). Therefore, the difference in slope between these two characteristics does not represent the true variation of slope. This difference was used only as an indication of the error involved in assumption (1). This error analysis is summarized in table 2. For weak shocks, assumption (1) is nearly exact for the complete range of the rarefaction wave; however, for a very strong shock, the deviation becomes excessive for regions past the midpoint of the rarefaction wave.

Assumption (2) states that the particle velocity remains constant along any characteristic within the rarefaction wave. To check the accuracy of the assumption, the graphical solution by the stepwise characteristics method was applied to three different initial strength shocks. The change in particle velocity along selected characteristic lines, positioned at various percentages of particle velocity decrease behind the head of the rarefaction wave, was calculated by the graphical characteristics method and is listed in table 3. It should be noticed that assumption (2) is reasonably accurate even for shocks which are initially very strong. From the data, one may conclude that the motion of the shock front is described with reasonable accuracy by the present analytical solution for shocks of strength $\frac{p_2 - p_1}{p_1} < 6$.

2. Comparison of Solutions

In this section, comparisons are made among results obtained from the three methods, namely,

1) weak shock solution, by Friedrichs

2) present analytical solution

3) graphical solution by the method of characteristics.

Figure 4 represents the time-displacement curves for shock fronts of initially different strengths attenuated by rarefaction waves. For weak shocks, all methods yield similar results for the shock path as shown in figure 4a. For strong shocks, figure 4b, both the graphical solution and the present analytical solution produce similar results until the shock strength equals approximately one half of its original value. The weak shock approximation, on the other hand, contains considerable error for a shock of this strength. For very strong shocks, figure 4c, the present analytical solution and the graphical solution are in close agreement until the shock strength equals about 2/3 of its original value. The weak shock approximation is plotted in figure 4c for comparison. At this shock strength, the weak shock approximation is not mathematically consistant. The pressure distribution along a constant time line behind the strong shock front as computed by the three methods is illustrated in figure 5. With the present analytical solution, it is not possible to calculate the complete pressure distribution behind the shock front. However, the pressure may be calculated at two points;

1) directly behind the shock front, and

2) at the tail of the rarefaction wave.

As a rough approximation to the pressure, a linear distribution between these two points is assumed. This approximation to the pressure agrees reasonably well with the graphical solution, see figure 5. The small pressure discontinuities in

the graphical solution are caused by the reflected waves which originate at the shock-rarefaction interactions.

Figure 6 represents the decrease in propagation velocity of a decaying strong shock as calculated by the three methods. The pressure decay is illustrated in figure 7.

VI. Behavior of Weak Shocks at Large Values of Time according to Approximate Solutions

According to Friedrichs' approximation for weak shocks, the distance between the shock front and the tail of the rarefaction wave i.e., the "width of the shock wave," increases according to the square root of time for large values of time. With our present analytical approximation, the "width of the shock wave" reduces to zero since the shock and rarefaction tail intersect at some finite large time. Thus, using the present approximation procedure, the shock front ends at some finite time. The difference between these two approximate solutions is shown schematically in figure 8.

The disagreement between the two solutions can be attributed to a difference in both the location of the rarefaction wave and the position of the shock front. In both approximations, the tail of the rarefaction wave is a straight line in the x-t plane, (see figure 8). By Friedrichs' method, in which the entropy change across the shock front is neglected, the fluid properties at the tail of the rarefaction wave are identical with the properties of the undisturbed fluid, and the slope of the tail is $1/c_1$. However, the present approach considers the entropy change across the shock front. Therefore, the pressure and sound speed at the tail of the rarefaction wave are both slightly larger than the values in the undisturbed region, and the slope of the tail is $1/c_3$ where $1/c_3 < 1/c_1$.

The exact slope of the rarefaction tail before it is effected by the reflected wave system (region 3 of figure 2) is $1/c_3$. Thus, the present approximation gives the correct location of the initial portion of the tail of the rarefaction wave. At large values of time, the strength of the shock front deteriorates, and the slope of the tail must approach $1/c_1$. Therefore, Friedrichs' approximation gives the correct slope of the tail at large values of time. The tail must lie between these two straight lines as shown in figure 8, although its exact location is not known.

The path of the shock front in the x-t plane calculated by the present method always lies above the shock calculated by Friedrichs' method. This difference in location occurs not only because of Friedrichs' isentropic assumption but also because of his approximate expression for shock velocity (see appendix B).

The above differences cause the solutions to conflict at large values of time. Unfortunately, the exact position of the shock path is not known. The question whether, at large values of time, the "width of shock" reduces to zero, approaches a constant, or increases monotonically is still unanswered.

VII. Concluding Remarks

The approximate analytical expression for the path of a decaying strong plane shock in an ideal gas is developed in the body of this report. Such a solution is significant since no exact analytical solution to the problem exists, and numerical solutions of the characteristic equations in finite-difference form are too lengthly. The solution as presented is based upon certain simplifying assumptions considered in Section IV-2. These assumptions introduced very little error in the early stage of the shock front because the rarefaction wave has not yet undergone many deflections caused by the shock-rarefaction interactions. From the analytical solution, equations for the pressure and velocity decay of a shock wave are developed.

Because of the absense of an exact analytical solution, a solution to the shock attenuation problem was also carried out graphically by the method of characteristics. A new procedure was developed in this phase which facilitated the otherwise lengthy calculations inherent in the step-wise characteristics method. The modified graphical method for this particular problem utilizes the $(p/p_1)^{\frac{\gamma-1}{2\gamma}}$ vs. u/c_1 state plane. This step-wise characteristics method then comprised the basis of comparison for the approximate analytical solution.

The results of the two solutions (analytical and graphical) are comparable in the early stages of shock front propagation. The accuracy of the approximate analytical solution, as compared with that of the graphical solution, decreases for later stages of strong shock front propagation.

These solutions were also compared with an approximate solution for weak shocks by Friedrichs. For weak shocks, all three solutions agree in the early stages of the wave motion; however, a significant difference exists between the present analytical solution and Friedrichs' solution at very large values of time.

By a modification of the equation of state, the approximation technique developed in this report can be extended to other media. Regarding the solution of the spherical shock problem in water, the next phase of this project will be to study (by the methods developed in this report) the decay of a strong plane shock in water. Following this study, an investigation of the spherical shock problem will be undertaken. Although only one space coordinate is required to describe the position of the shock front, the area of the spherical shock front is not constant. Therefore, a modification of the present stepwise method of characteristics will be required.

The apparent accuracy of our approximation procedure, for one-dimensional unsteady strong shocks, suggests a possible extension of the method into other problems of one-dimensional unsteady gas motion and two-dimensional steady motion. For example, those problems studied by Friedrichs in reference (7), such as the decay of shocks in two-dimensional steady flow and decaying n-waves, may be extended to include the strong shock range.

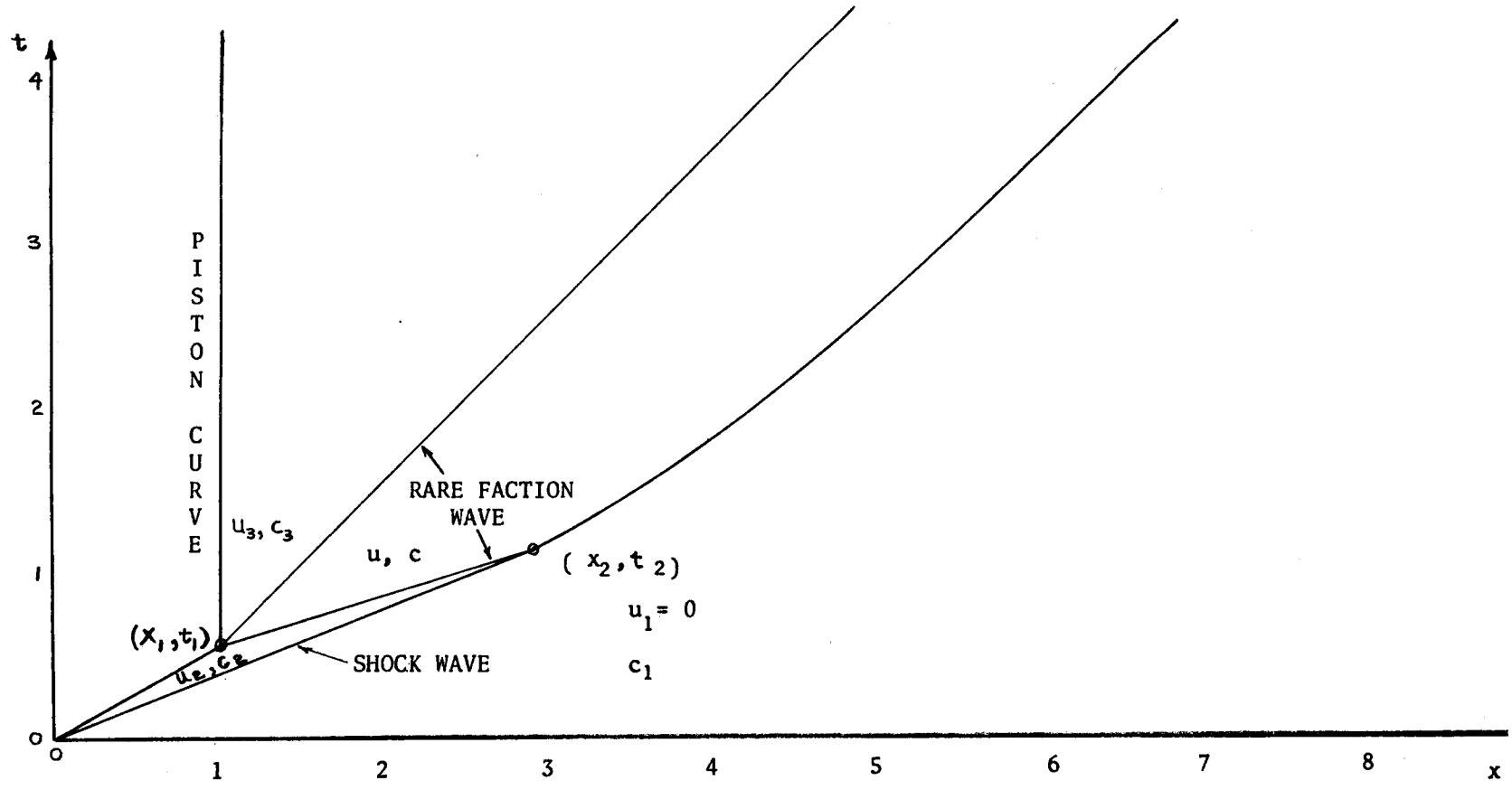

FIGURE 1. SHOCK FRONT OVERTAKEN BY RAREFACTION WAVE - PHYSICAL PLANE

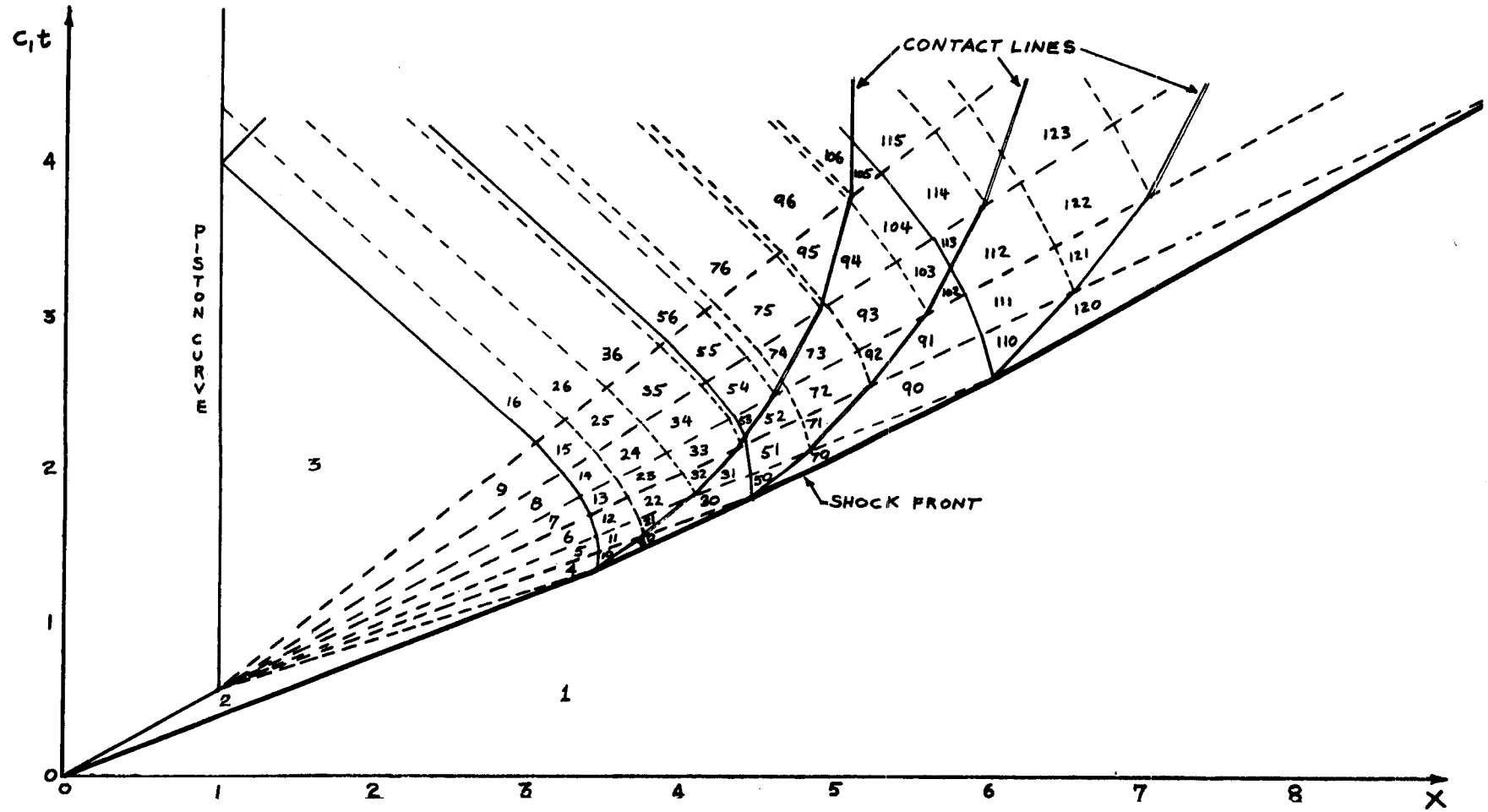

FIGURE 2. REGIONS IN THE PHYSICAL PLANE USED IN THE STEPWISE CHARACTERISTICS METHOD. (Problem 2., See Table 1 for state properties)

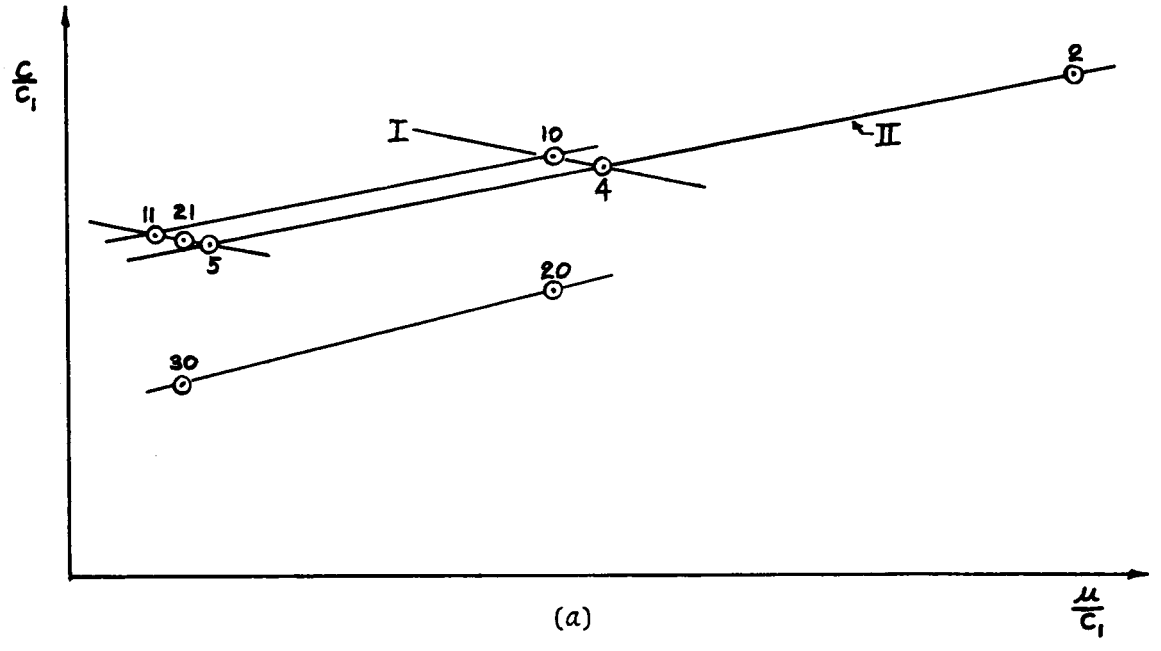

(a)

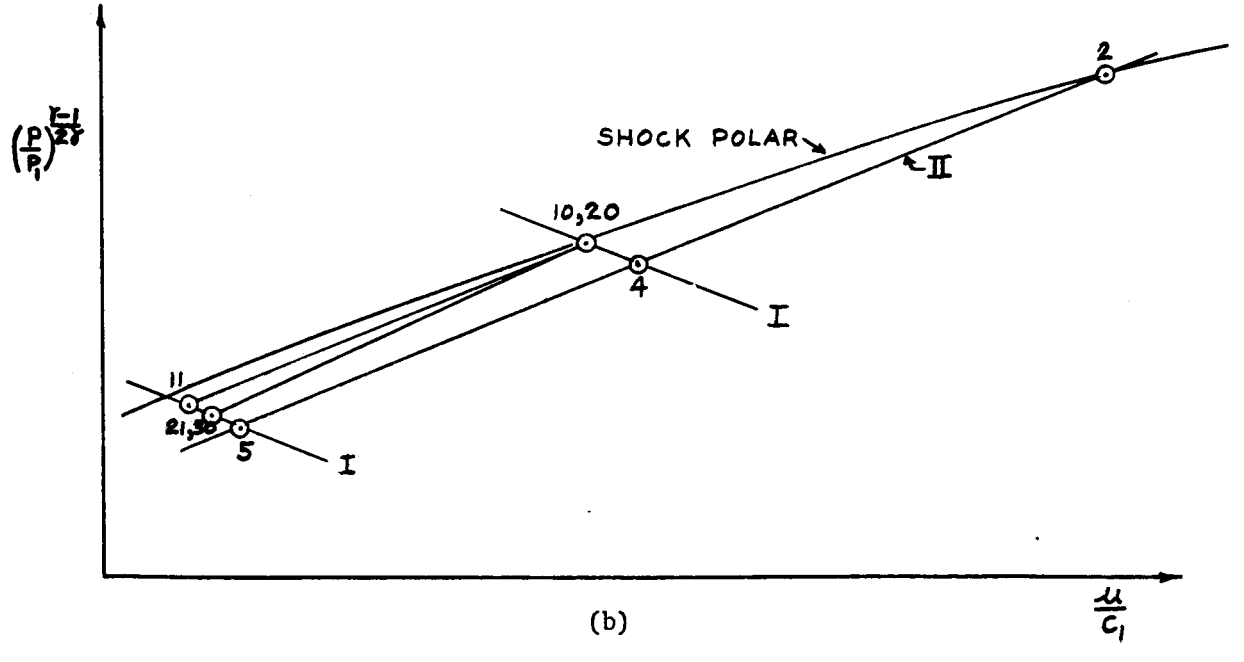

(b)

FIGURE 3. STATE PLANES

(a) $\frac{c}{c_1}$ versus $\frac{u}{c_1}$ state plane

(b) $\left(\frac{p}{p_1}\right)^{\frac{\gamma-1}{2\gamma}}$ versus $\frac{u}{c_1}$ state plane

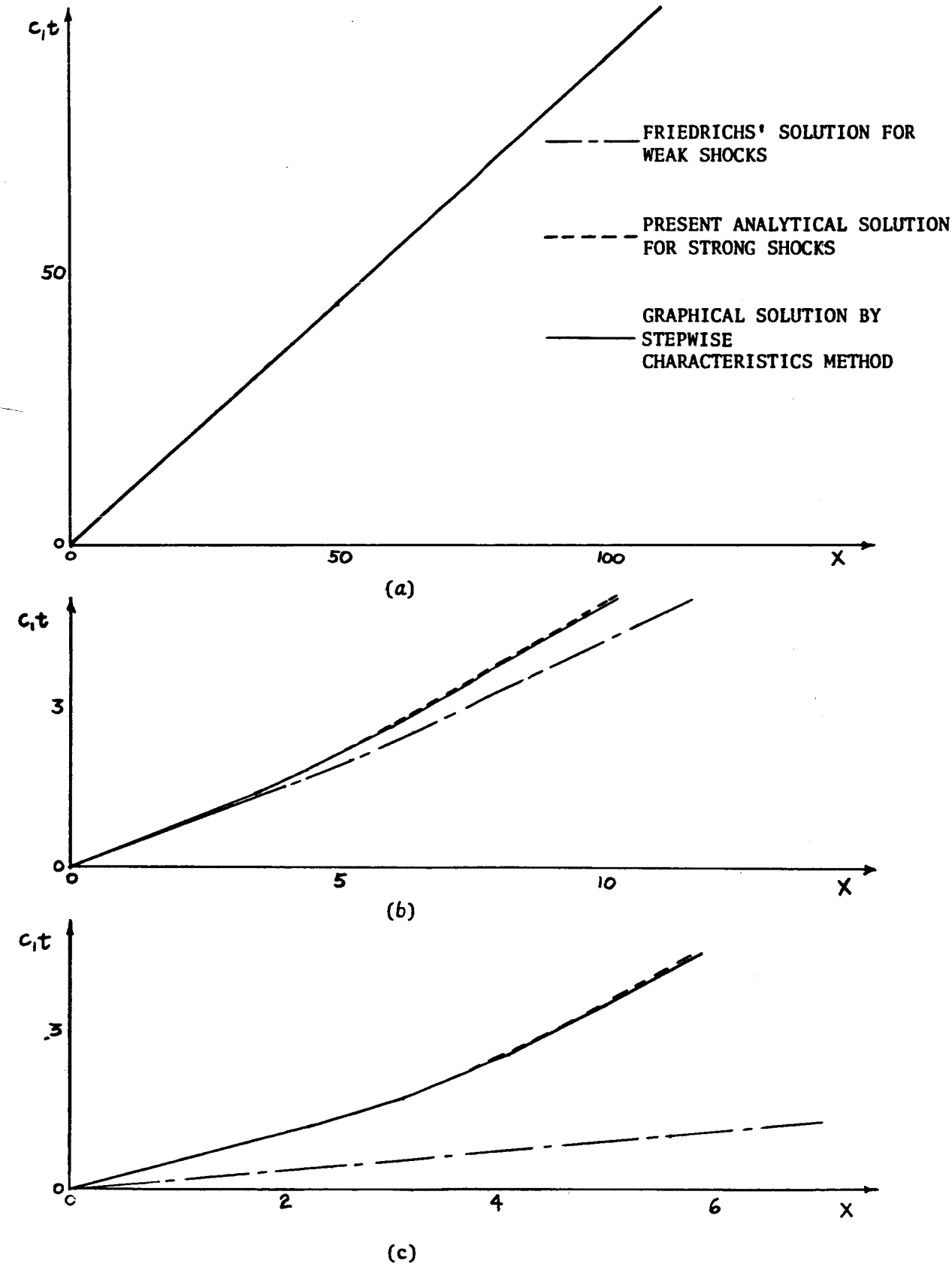

FIGURE 4. COMPARISON OF SOLUTIONS

(a) weak shock, initial excess pressure ratio $\frac{P_2-P_1}{P_1} = .274$

(b) strong shock, initial excess pressure ratio = 6.264

(c) very strong shock, initial excess pressure ratio= 428.9

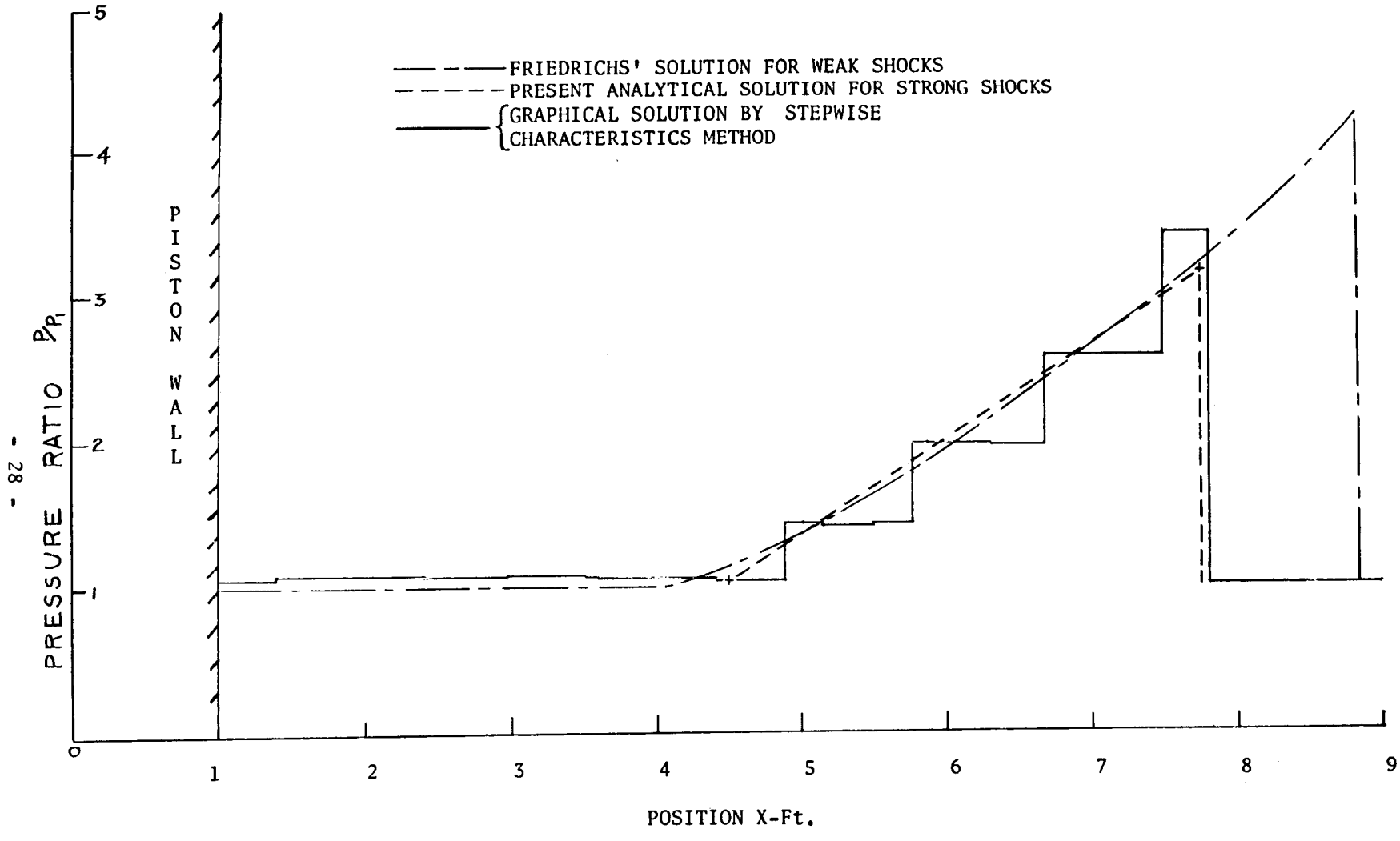

FIGURE 5. PRESSURE DISTRIBUTION BEHIND SHOCK FRONT AT TIME $C_1 t$ = 3.63 FOR A STRONG SHOCK.

INITIAL SHOCK STRENGTH $\frac{p_2 - p_1}{p_1}$ = 6.264

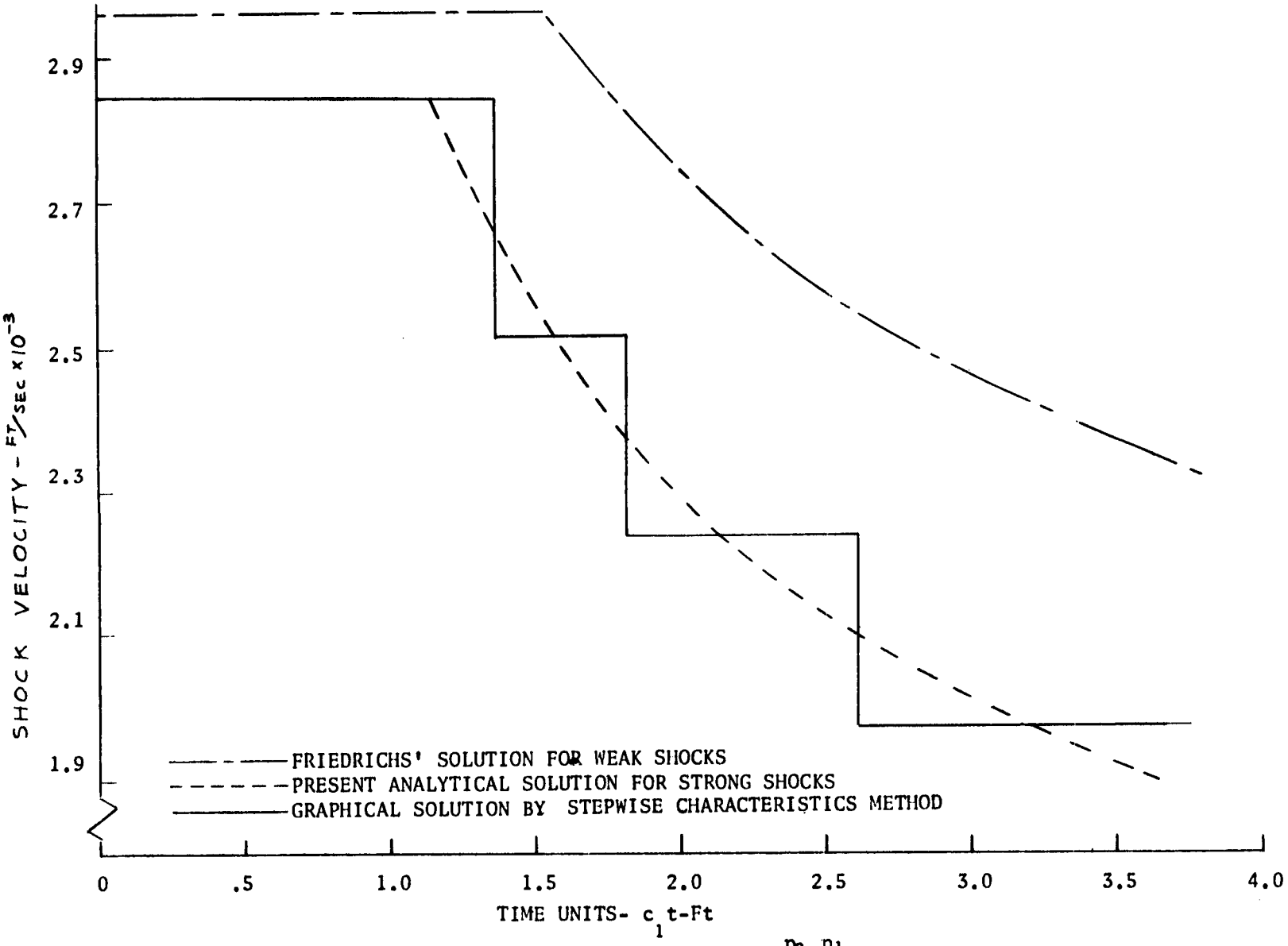

FIGURE 6. SHOCK VELOCITY DECAY FOR A STRONG SHOCK $\frac{p_2 \; p_1}{p_1} = 6.264$

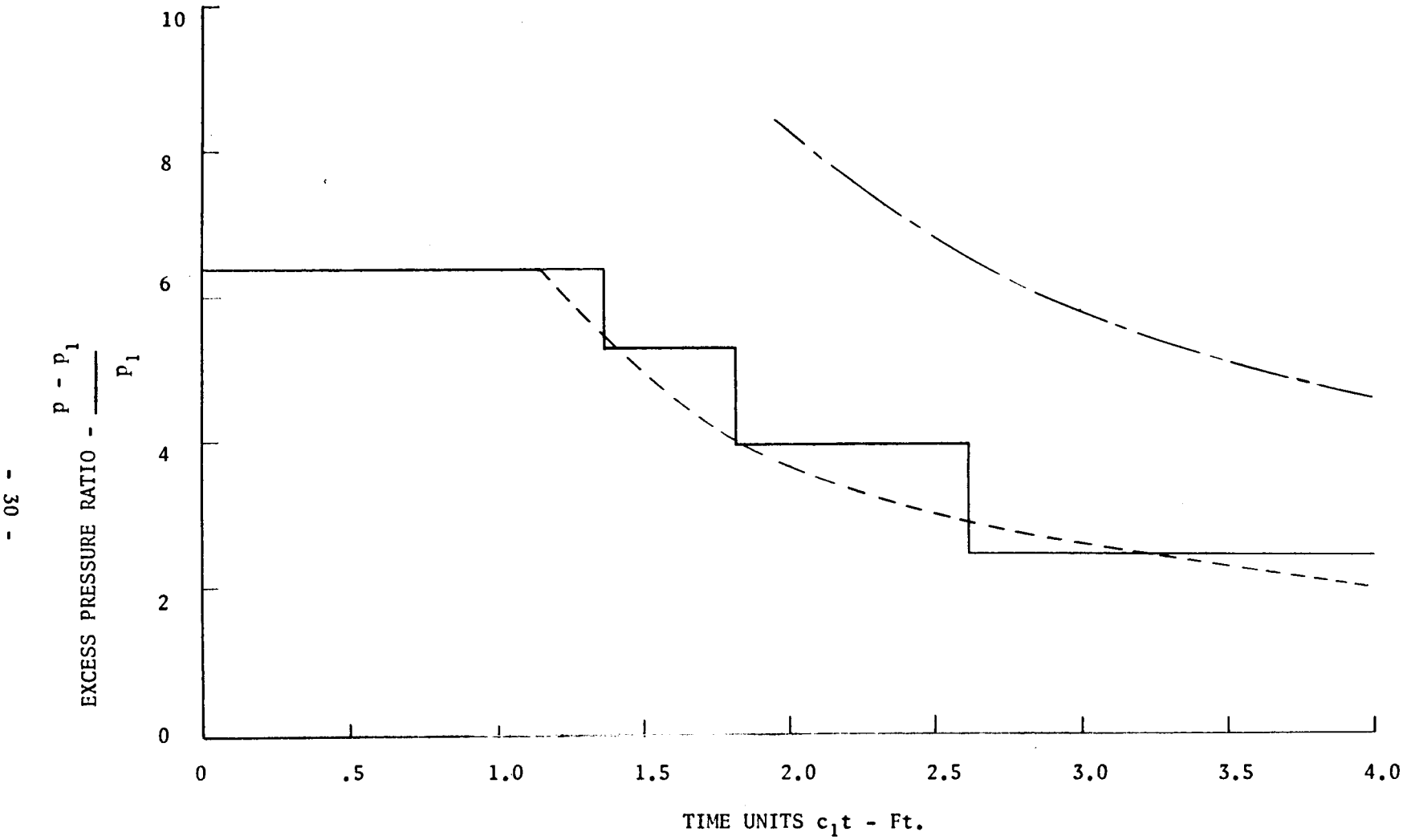

FIGURE 7. PRESSURE DECAY FOR A STRONG SHOCK $\frac{p_2 - p_1}{p_1} = 6.264$

——— - ——— FRIEDRICHS' SOLUTION FOR WEAK SHOCKS

- - - - - - - PRESENT ANALYTICAL SOLUTION FOR STRONG SHOCKS

——————— GRAPHICAL SOLUTION BY STEPWISE CHARACTERISTICS METHOD

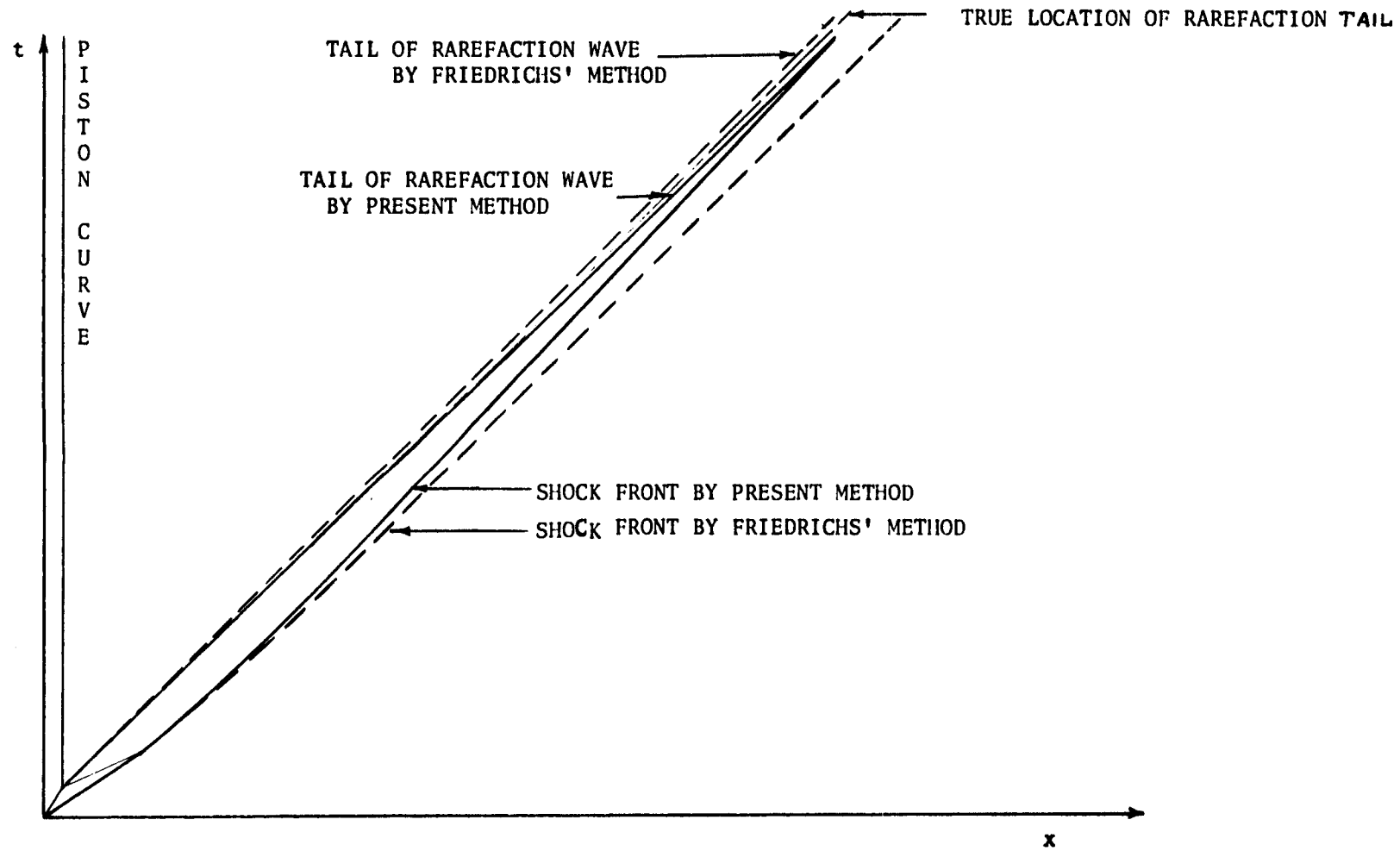

FIGURE 8. BEHAVIOR OF WEAK SHOCKS AT LARGE VALUES OF TIME (SCHEMATIC)

REGION	c/c_1	u/c_1	p/p_1
1	1	0	1
2	1.472	1.773	7.264
3	1.117	0	1.051
4	1.418	1.500	5.569
5	1.367	1.250	4.267
6	1.318	1.000	3.347
7	1.268	.750	2.552
8	1.217	.500	1.748
9	1.168	.250	1.435
10	1.421	1.483	5.705
11	1.371	1.234	4.419
12	1.321	.981	3.399
13	1.270	.736	2.586
14	1.221	.481	1.961
15	1.171	.230	1.463
16	1.120	-.015	1.070
20	1.373	1.483	5.640
21	1.370	1.242	5.529
22	1.319	.986	3.347
23	1.270	.741	2.586
30	1.324	1.242	4.371
31	1.275	.990	3.359
32	1.318	.990	3.347
33	1.269	.742	2.567
50	1.325	1.231	4.411
51	1.276	.982	3.378
52	1.227	.738	2.568
70	1.294	1.231	4.415
71	1.275	.990	3.353
72	1.226	.745	2.553
90	1.246	.990	3.378
91	1.197	.748	2.552
110	1.248	.984	3.422
111	1.200	.738	2.595
120	1.223	.984	3.434

TABLE 1--PARTIAL LIST OF STATE PROPERTIES

(Regions Correspond to Figure 2)

initial data: $u_1 = 0$, $c_1 = 1128$ ft/sec, $p_1 = 1$ atm

$u_2 = 2000$ ft/sec, $\gamma = 1.4$, piston travel $x_1 = 1$ ft.

Initial Shock Strength, Excess Pressure Ratio $\frac{p_2 - p_1}{p_1}$	Position within Rarefaction wave	Approximate Deviation In Slope of Characteristic Lines $\frac{s_1 - s_2}{s_1}$ %
weak	Head ($u = u_2$)	0
.274	Middle ($u = 1/2\ u_2$)	.014
	Tail ($u = o$)	.019
Strong	Head	0
6.264	Middle	4.28
	Tail	10.35
Very Strong	Head	0
428.9	Middle	17.1
	Tail	81.2

TABLE 2

MAGNITUDE OF ERROR IN SLOPE CAUSED BY ASSUMING

THE CHARACTERISTICS ARE STRAIGHT LINES.

s_1 = slope of characteristic directly behind shock front

s_2 = slope of characteristic within simple rarefaction wave

Note: Both characteristics have the same particle velocity

Initial Shock Strength, Excess Pressure Ratio $\frac{p_2 - p_1}{p_1}$	Position Within Rarefaction Wave-- Percent behind Head of Wave $\frac{u_2 - u}{u_2}$ %	Change in Particle Velocity Along A Characteristic line $\frac{u_B - u_s}{u_s}$
Weak	12.5	-0.38
.274	25	-0.43
Strong	15	-1.13
6.264	30	-1.52
	44	-1.60
Very Strong		
428.9	17	-1.90
	34	-2.60

TABLE 3

CHANGE IN PARTICLE VELOCITY ALONG A CHARACTERISTIC

OBTAINED BY GRAPHICAL (CHARACTERISTICS) SOLUTION

u_2 = piston velocity

u = particle velocity at position of interest within rarefaction wave

u_B = particle velocity directly behind shock

u_s = particle velocity within simple rarefaction wave

IX. REFERENCES

1. Stepka, Franics S., and Morse, Robert C.
"Preliminary Investigation of Catastrophic Fracture of Liquid-Filled Tanks Impacted by High-Velocity Particles"
NASA Technical Note D-1537, May, 1963.

2. Chou, Pei Chi, Sidhu, Harbans S., and Karpp, Robert R.
"Analysis of Peak Pressure Generated in Water by High Velocity Impact"
Drexel Institute of Technology
Report No. 160-1, April, 1963.

3. Rae, W. J., and Kirchner, H. P.
"Final Report on a Study of Meteoriod Impact Phenomena"
Cornell Aeronautical Laboratory, Inc., Report No. RM-1655-M-4,
February, 1963.

4. Davids, Norman, and Huang, Y. K.
"Shock Waves in Solid Craters"
"Journal of The Aerospace Sciences", Vol. 29, No. 5, May, 1962.

5. Herrmann, Walter, Witner, Emmett A., Percy, John H., and Jones, Arfon H.,
"Stress Wave Propagation and Spallation in Uniaxial Strain" ASD-TDR-62-399, Air Force Systems Command, Wright-Patterson Air Force Base,
September, 1962.

6. Al'tshuler, L. V., Kormer, S. B., Brazhnik, M.I., Vladimirov, L.A., Speranskaza, M. P., and Funtikov, A. I., "The Isentropic Compressibility of Aluminum, Copper, Lead, and Iron at High Pressures".
"Soviet Physics Jetp," Vol. 11, No. 4, October, 1960.

7. Friedrichs, K. O., "Formation and Decay of Shock Waves", "Communications on Pure and Applied Mathematics," 1948.

8. Lighthill, M.J., "The Energy Distribution behind Decaying Shocks,"
Philosphical Magazine, Vol. 41, Nov. 1950.

9. Fowles, G. R., "Attenuation of the Shock Wave Produced in a Solid by A Flying Plate," Journal of Applied Physics, Vol. 31, No. 4., April, 1960.

10. Courant, R., and Friedrichs, K. O., "Supersonic Flow and Shock Waves"
Interscience Publishers, Inc., New York, 1948.

11. Shapiro, Ascher H., "The Dynamics and Thermodynamics of Compressible Fluid Flow", Vol. II., The Ronald Press Co., New York, 1954.

X. NOTATIONS:

u	gas particle velocity
U	shock propagation velocity
c	sound speed
γ	specific heat ratio
ρ	density
p	pressure
t	time
x	displacement

Subscript 1	Signifies conditions ahead of the shock
Subscript 2	Signifies conditions behind the initial portion of the shock

APPENDIX A

Behavior of the Shock Polar and Characteristic Lines in the State Planes

In applying the graphical method, since frequent use is made of the shock polar and the state characteristic lines, it is desirable to establish their behavior in the state planes. A discussion of the behavior of the shock polar and characteristic lines in the p/p_1 vs. u/c_1 plane and in the $(p/p_1)^{\frac{\gamma-1}{2\gamma}}$ vs. u/c_1 plane will be given. The behavior of these curves in the c-u state plane is discussed in detail in reference [11], Chapter 25. The state planes are shown in figure A.

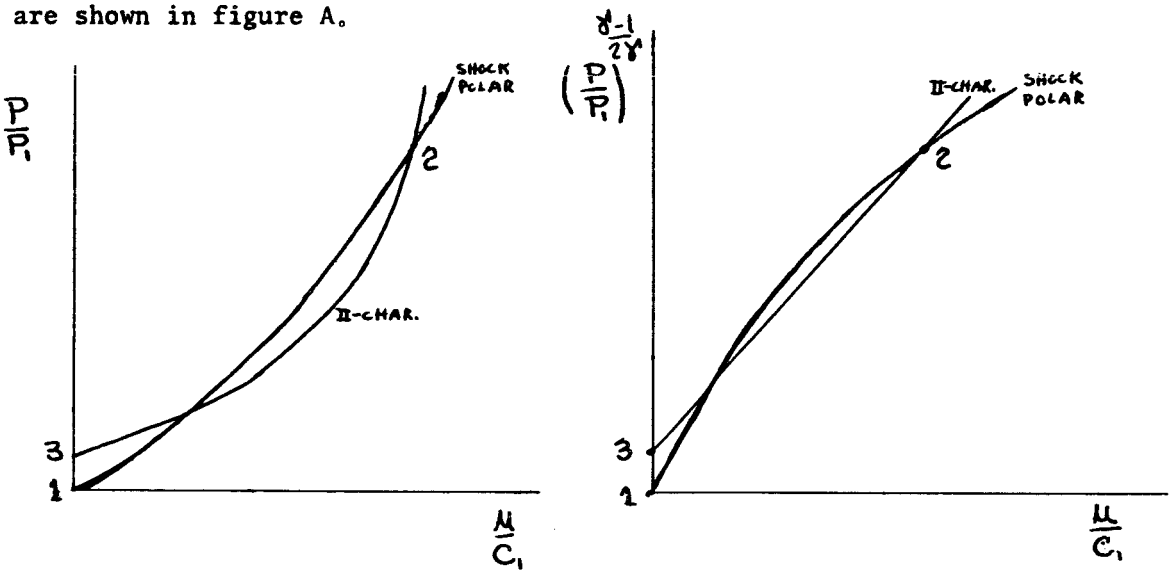

FIGURE A

In both the p/p_1 vs. u/c_1 plane and the $(p/p_1)^{\frac{\gamma-1}{2\gamma}}$ vs. u/c_1 plane, a II-characteristic is shown to intersect the shock polar at two points. One intersection is at point 2, which corresponds to the state of a region immediately behind the shock front. It will be shown that another intersection exists.

It will first be shown that, at point 2 where isentropic expansion begins, the slope of the II-characteristic is greater than the slope of the shock polar. Hence, part of the characteristic curve must lie below the shock polar, as shown

in figure A. Proof of at least one other intersection will be established by showing that, at the vertical axis, $p_3 > p_1$. The following proof refers to the p/p_1 vs. u/c_1 state plane.

The equations for the shock polar and characteristics are respectively,

$$\frac{u}{c_1} = \frac{\left(\frac{p}{p_1} - 1\right)}{\gamma\left[\left(\frac{p}{p_1} - 1\right)\frac{\gamma+1}{2\gamma} + 1\right]^{1/2}} \tag{A.1}$$

and

$$\frac{p}{p_1} = \left(\frac{p_2}{p_1}\right)\left(\frac{c_1}{c_2}\right)^{\frac{2\gamma}{\gamma-1}}\left[\frac{c_2}{c_1} + \frac{\gamma-1}{2}\left(\frac{u}{c_1} - \frac{u_2}{c_1}\right)\right]^{\frac{2\gamma}{\gamma-1}} \tag{A.2}$$

The slope of the shock polar is

$$\frac{d\left(\frac{p}{p_1}\right)}{d\left(\frac{u}{c_1}\right)} = 2\gamma\frac{\left[\left(\frac{p}{p_1} - 1\right)\frac{\gamma+1}{2\gamma} + 1\right]^{3/2}}{\left[\left(\frac{p}{p_1} - 1\right)\frac{\gamma+1}{2\gamma} + 2\right]}, \tag{A.3a}$$

and the slope of the characteristic is

$$\frac{d\left(p/p_1\right)}{d\left(u/c_1\right)} = \gamma\left(\frac{c_1}{c_2}\right)\left(\frac{p_2}{p_1}\right)^{\frac{\gamma-1}{2\gamma}}\left(\frac{p}{p_1}\right)^{\frac{\gamma+1}{2\gamma}} \tag{A.4a}$$

where subscript 2 refers to the region immediately behind the shock. To determine the slope of the characteristic at the point of intersection, point 2 in figure A, p is equal to p_2 and equation (A. 4a) becomes

$$\frac{d\left(\frac{p}{p_1}\right)}{d\left(u/c_1\right)} = \gamma\left(\frac{c_1}{c_2}\right)\left(\frac{p_2}{p_1}\right) \tag{A.4b}$$

To determine c_1/c_2 as a function of the pressure ratio p_2/p_1, the following shock relations are used.

$$\frac{p_2}{p_1} = 1 + \frac{2\gamma}{\gamma+1}\left[\left(\frac{u}{c_1}\right)^2 - 1\right] \tag{A.5}$$

and

$$\left(\frac{c_2}{c_1}\right)^2 = 1 + \frac{2(\gamma-1)}{(\gamma+1)^2}\left[\gamma\left(\frac{u}{c_1}\right)^2 - \left(\frac{c_1}{u}\right)^2 - (\gamma-1)\right] \tag{A.6}$$

Solving for U/c_1 from equation (A.5) and substituting it into equation (A.6),

one obtains

$$\left(\frac{c_2}{c_1}\right)^2 = 1 + \frac{2(\gamma-1)}{(\gamma+1)^2}\left[\gamma\left\{\frac{\gamma+1}{2\gamma}\left(\frac{P_2}{P_1}-1\right)+1\right\} - \frac{1}{\frac{\gamma+1}{2\gamma}\left(\frac{P_2}{P_1}-1\right)+1}^{-(\gamma-1)}\right] \quad \text{(A.7a)}$$

To simplify the following equations, γ is set equal to 1.4. Equation (A.7a) then becomes

$$\left(\frac{c_2}{c_1}\right)^2 = \frac{\left(\frac{P_2}{P_1}\right)\left(\frac{P_2}{P_1}+6\right)}{6\left(\frac{P_2}{P_1}\right)+1} \quad \text{(A.7b)}$$

By substituting equation (A.7a) into (A.4b), the slope of the characteristic at point 2, may be expressed as a function of p_2 / p_1.

$$\left.\frac{d\left(\frac{P_2}{P_1}\right)}{d\left(\frac{u}{c_1}\right)}\right|_{P=P_2} = 1.4\left(\frac{P_2}{P_1}\right)\left[\frac{6\left(\frac{P_2}{P_1}\right)+1}{\left(\frac{P_2}{P_1}\right)\left(\frac{P_2}{P_1}+6\right)}\right]^{1/2} \quad \text{(A.8)}$$

The slope of the shock polar, equation (A.3a), with $\gamma = 1.4$ is

$$\frac{d\left(\frac{P_2}{P_1}\right)}{d\left(u/c_1\right)} = 2.8\,\frac{\left[\left(\frac{P_2}{P_1}-1\right)\frac{6}{7}+1\right]^{3/2}}{\left[\left(\frac{P_2}{P_1}-1\right)\frac{6}{7}+2\right]} \quad \text{(A.3b)}$$

Let R represent the ratio of the slope of the characteristic to the slope of the shock polar at point 2, or

$$R = \frac{\left(\frac{P_2}{P_1}\right)\left[\frac{6\left(\frac{P_2}{P_1}\right)+1}{\left(\frac{P_2}{P_1}\right)\left(\frac{P_2}{P_1}+6\right)}\right]^{1/2}}{2\,\frac{\left[\left(\frac{P_2}{P_1}-1\right)\frac{6}{7}+1\right]^{3/2}}{\left[\left(\frac{P_2}{P_1}-1\right)\frac{6}{7}+2\right]}} \quad \text{(A.9)}$$

Equation (A.9) may be simplified into the following inequality,

$$R > \left[1 + \frac{27\left(\frac{P_2}{P_1}\right)^3 - 60\left(\frac{P_2}{P_1}\right)^2 + 39\left(\frac{P_2}{P_1}\right) - 6}{36\left(\frac{P_2}{P_1}\right)^3 + 228\left(\frac{P_2}{P_1}\right)^2 + 73\left(\frac{P_2}{P_1}\right) + 6}\right]^{1/2}$$

Numerical calculations show that for any value of p_2 / p_1 greater than one, R is also greater than one. Also, it can be shown numerically that R is greater than one for any γ greater than 1.1. The above ratio illustrates that one part of the characteristic must lie below the shock polar.

The expansion portion of the characteristic will cross the shock polar again if the final pressure p_3 is greater than the initial pressure p_1, or, if $p_3 / p_1 > 1$. From equation (A.2), with u= o and p= p_3, one obtains

$$\frac{P_3}{P_1} = \frac{P_2}{P_1}\left[1 - \frac{\gamma-1}{2}\frac{u_2}{c_2}\right]^{\frac{2\gamma}{\gamma-1}} \tag{A.10}$$

The pressure ratio p_3 / p_1 may be obtained as a function of U/c_1 by combining equations (A.5), (A.6), and (A.9).

$$\frac{P_3}{P_1} = \left[1 + \frac{2\gamma}{\gamma+1}\left(\left(\frac{u}{c_1}\right)^2 - 1\right)\right]\left\{1 - \left(\frac{\gamma-1}{\gamma+1}\right)^2\left[\frac{\left(\frac{u}{c_1} - \frac{c_1}{u}\right)^2}{1 + \frac{2(\gamma-1)}{(\gamma+1)^2}\left[\gamma\left(\frac{u}{c_1}\right)^2 - \left(\frac{c_1}{u}\right)^2 - (\gamma-1)\right]}\right]\right\}^{\frac{2\gamma}{\gamma-1}} \tag{A.11}$$

Numerical calculations of equation (A.11) show that $p_3 / p_1 > 1$ for any $U/c_1 > 1$ and for γ equal to or greater than 1.1. Hence, the lower part of the characteristic lies above the shock polar which indicates at least one other intersection.

APPENDIX B

Relative Positions of Shock Paths According to the Two Approximations

In Section VI, it is stated that, for the same initial conditions, the shock path in the x-t plane calculated from Friedrichs' equation lies below the path calculated from the present equations. There are two factors which contribute to this difference:

1) Friedrichs utilized an approximate equation for the shock velocity as a function of particle velocity u. It will be shown that the values of shock velocity U given by this approximate equation are larger than the values given by the exact equation at the same u. The slope of the shock path is 1/U; therefore, the shock path given by the approximate equation has a smaller slope than that given by the exact equation.

2) The rarefaction wave calculated by Friedrichs' method is propagated at a slower rate than that calculated by the present method. Therefore, the rarefaction wave calculated by the present method overtakes the shock and decreases its velocity more rapidly; consequently, the shock path according to the present approximation lies above that of Friedrichs'.

Proof of 1:

The exact shock equation (U= f (u)) used in the present method is

$$\frac{U}{c_1} = \frac{\gamma+1}{4}\mu + \sqrt{\left(\frac{\gamma+1}{4}\right)^2\mu^2 + c_1^2} \qquad (B.1)$$

The approximate equation used in Friedrichs' method is

$$\frac{U}{c_1} = 1 + \frac{1}{2}\sigma + \frac{1}{8}\sigma^2, \qquad (B.2)$$

where $$\sigma = \frac{\gamma+1}{2}\frac{\mu}{c_1} < 1 \quad .$$

The exact shock relationship in terms of σ is

$$\frac{U}{C_1} = \frac{\sigma}{2} + \sqrt{\frac{\sigma^2}{4} + 1} \qquad \text{(B.3)}$$

Equation (B.3) can be expanded into

$$\frac{U}{C_1} = 1 + \frac{\sigma}{2} + \frac{\sigma^2}{8} - \frac{1}{2\cdot4}\left(\frac{\sigma^2}{4}\right)^2 + \frac{1\cdot3}{2\cdot4\cdot6}\left(\frac{\sigma^2}{4}\right)^2 - \cdots + \cdots \qquad \text{(B.4)}$$

Subtracting the approximate equation (B.2) from the exact equation (B.4), one finds that the remainder is a negative quantity since the magnitude of each negative term is larger than the subsequent positive term, i.e.,

$$-\frac{1}{2\cdot4}\left(\frac{\sigma^2}{4}\right)^2\left[1 - \frac{3}{6}\left(\frac{\sigma}{4}\right)\right] < 0 \quad .$$

This analysis illustrates that, for the same u_p the value of U given by the approximate equation is larger than the value given by the exact equation.

Proof of 2:

Reference 11, page 1006 illustrates that, for $\gamma = 1.4$, the slope of the shock polar in the u-c plane is always greater than or equal to the slope of a characteristic line. The typical slope of these curves is shown below.

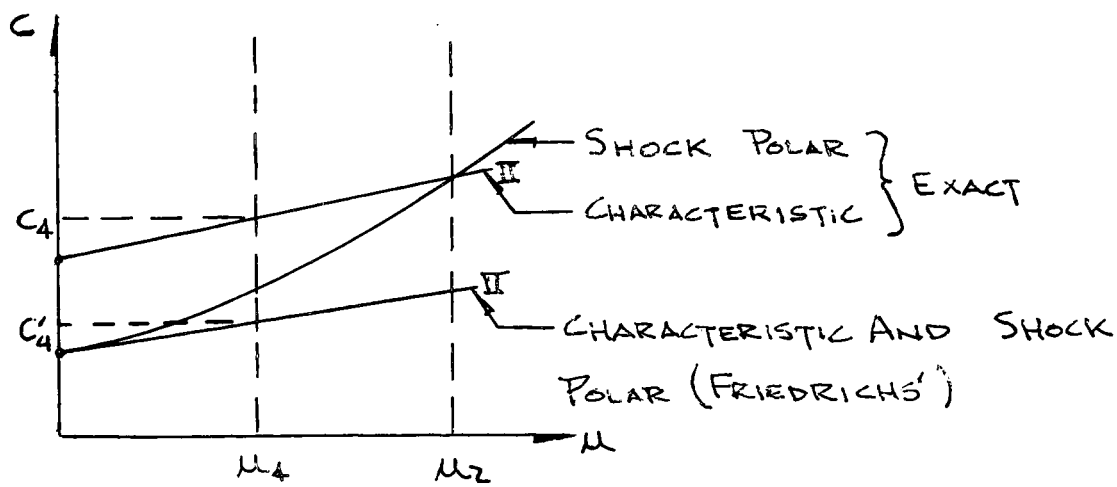

Consider a shock with the particle velocity u_2 behind it and an isentropic expansion from u_2 to a smaller particle velocity u_4. The figure shows that

the resulting sound speed c_4 is larger than c_4', where c_4' is obtained by assuming that the shock is an isentropic compression wave (Friedrichs' assumption). The characteristics within the rarefaction wave have velocities given by $u + c$; therefore, for a given value of u, the velocity of a characteristic given by Friedrichs' method is less than the velocity given by the present method.